Fermilab Summer School 2018

Fermilab

Final Report

Temperature Dependence of the Laser Calibration Signals in the Muon g-2 Experiment and Correction

Intern:
Francesco Carnevali

Supervisor:
Prof. Michele Iacovacci

Contents

Introduction

During the summer school at Fermilab I have worked on the Muon g-2
experiment. The work carried out provided both a hardware part and a
part of data analysis. I took part at the beginning of the installation of a
new crate for the local monitor of the laser calibration system and I tested
24 new preamplifiers. Data analysis investigated the correlation between
the Source Monitor signals and the preamplifier temperature. The signals,
in fact, turned out to be anticorrelated with the temperature and in order
to make these indipendent by external factors have been corrected, reducing
the induced fluctuations. The time range analyzed was 30 days long, the
largest so far. Thanks to this analysis we could observe electronic behaviors,
which were not shown in previous analysis. In fact, the electronics behaves
differently in two distinguishable regimes as a range of low temperatures
and high temperature ranges.

Chapter 1

The Muon g-2 Experiment

1.1 Introduction

Precision measurements of fundamental quantities played a key role in the development of the Standard Model. Although the latter, in fact, very well describes many phenomena, it is necessarily incomplete because it leaves some unexplained things.

The reason why the anomaly a_μ of the muon magnetic moment is so interesting in the view of the Standard Model is that it can be predicted very accurately by the theory and at the same time can be measured with great precision.

The purpose of the Muon g-2 experiment at Fermilab is to reduce the error on the anomaly from 0.54 ppm (BNL E821) to 0.14 ppm which is comparable with the 0.4 ppm uncertainty predicted by the Standard Model. In this way it is possible to increase the standard deviation from 3σ to 5σ which is the threshold for reaching a discovery.

Compared to previous experiments, some advances are necessary to achieve the required statistical uncertainty of 0.14 ppm. Among these improvements, the focus will be on continuous monitoring and recalibration of the detectors; in particular, a high precision laser calibration system will be used that will control the calorimeter gain fluctuation at 0.04% accuracy.

1.2 Theoretical prediction of the muon's anomaly

According to the Dirac theory a point-like charged elementary particle with spin $\frac{1}{2}$ has magnetic moment

$$\vec{\mu} = g\frac{q}{2m}\vec{S} \quad with\ g = 2 \tag{1.1}$$

Applying theoretical corrections due to QED, EW and QCD a value of $g > 2$ is obtained.
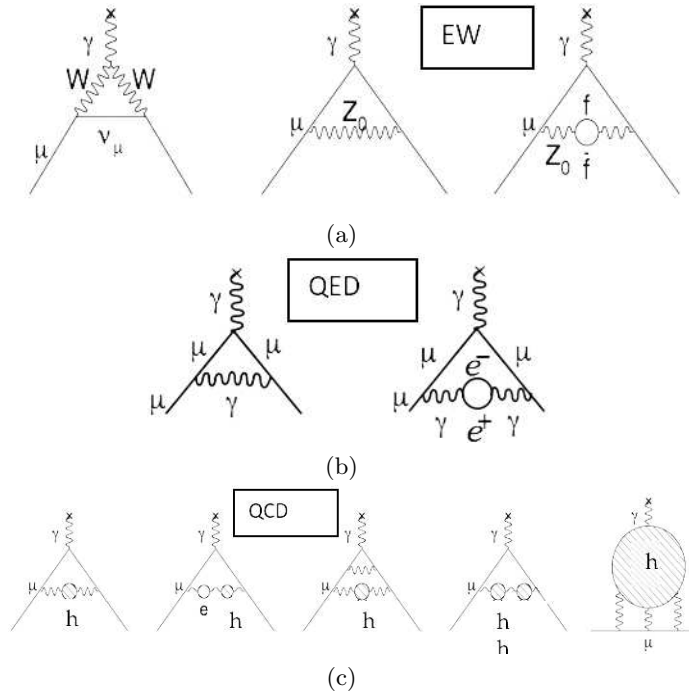

(a)

(b)

(c)

Figure 1.1: Feynman diagrams related to the theoretical corrections predicted by the Standard Model.

The quantity

$$a_\mu = \frac{g_\mu - 2}{2} \tag{1.2}$$

is defined as anomalous magnetic moment. The theoretical parameter obtained from the Standard Model theory is therefore composed of the sum of three factors: a term obtained with the QED (Quantum Electrodynamics), a term obtained with the EW (Electroweak Theory) and a term obtained with the QCD (Quantum Chromodynamics) . The QED parameter is derived from Feynman diagrams that describe the electromagnetic interaction muon-muon up to the fifth order of development in α, fine-structure con-

stant:

$$\alpha_\mu^{QED} = \frac{\alpha}{2\pi} + 0.7658577376 \left(\frac{\alpha}{2\pi}\right)^2 + 24.05050898 \left(\frac{\alpha}{2\pi}\right)^3 + 131.0 \left(\frac{\alpha}{2\pi}\right)^4 + 930.0 \left(\frac{\alpha}{2\pi}\right)^5$$

(1.3)

Assuming the latest measure of atomic interferometry for α

$$\alpha^{-1} = 137.036003(10) \tag{1.4}$$

the total contribution of α_μ given by the QED results

$$\alpha_\mu^{QED} = 1158471.96(12)(9) \times 10^{-10} \tag{1.5}$$

The uncertainty on this value is given by two contributions: the first is the estimated error corresponding to the perturbation approximation of the fifth order, while the second is due to the experimental error on the measure of α.

The contribution of the electroweak part is determined by the Feynman diagrams relating to the muon-muon interaction, through virtual exchanges of bosons $W_\pm$, Z or Higgs; the EW contribution is extremely less than the QED contribution. Ultimately, the parameter calculated through the electroweak theory is:

$$\alpha_\mu^{EW} = 15.4(1)(2) \times 10^{-10} \tag{1.6}$$

where the first error is the theoretical estimate due to the perturbative approximation, while the second term is related to the uncertainty on the mass of the Higgs.

The contribution of QCD is the one with the biggest computational complexity, since in low energy it is not possible to use QCD in a perturbative way and therefore the same calculation can not be performed as in the case of the terms of QED and EW. In fact, at low energies, there are phenomena of the synchronization of quarks that can be treated only through phenomenological models. The contribution due to HVP (Hadrons Vacuum Polarization) can be expressed through the formula:

$$\alpha_\mu^{HVP} = \frac{1}{3} \left(\frac{\alpha}{2\pi}\right)^2 \int_{4(\pi)^2 m}^{\infty} \frac{R(s)}{s} K(s) ds \tag{1.7}$$

where $K(s)$ is the kernel of QED and R(s) is experimentally determined as

$$\frac{\sigma(e^+ e^- \rightarrow hadrons)}{\sigma(e^+ e^- \rightarrow \mu^+ \mu -)} \tag{1.8}$$

HVP estimates therefore result

$$\alpha_\mu^{HVP} = (693.4 \pm 5.3 \pm 3.5) \times 10^{-10} \tag{1.9}$$

where the first error is of statistical type, the second one derives from the radiative type corrections. This contribution is mainly given by the formation of the pair $\mu^+\mu^-$; the formation of other hadrons makes less important contributions as at low energies $\mu^+\mu^-$ is the minor mass pair. The total theoretical estimate obtained by adding all the contributions is:

$$a_\mu^{SM} = a_\mu^{QED} + a_\mu^{EW} + a_\mu^{QCD} = (11659183.0 \pm 6.3 \pm 3.5 \pm 0.3) \times 10^{-10} \quad (1.10)$$

The E821 experiment (BNL) in Brookhaven measured

$$a_\mu^{Expt} - a_\mu^{SM} = (260 \pm 78) \times 10^{-11} \qquad 3.4\sigma \qquad (1.11)$$

The goal is to bring 3.4σ to 5σ reducing systematic and statistical errors. If the gap was stored it would be a further confirmation of the existence of a new physics beyond the standard model.

$$a_\mu^{Expt} = a_\mu^{SM} + a_\mu^{NewPhysics} \qquad (1.12)$$

In order to measure the anomaly of the gyromagnetic factor two elements essentially serve: the decay of the pion and the muon. As for the first process $\pi^- \to \mu^- + \bar\nu_\mu$, since the pion is a spin 0 boson, in the decay, the spins of the muon and of the muon neutrino must be opposed. Moreover, in the system of the center of mass of the pion, for the conservation of the momentum, the muon and the muon antineutrino have parallel and discordant impulses. Because the helicity of $\bar\nu_\mu$ is +1 and the spin of π^- is 0, the μ^- spin and the momentum are parallel and concordant and the elicity is +1. It is known, however, that massless leptons have a helicity of -1, so in theory the decay is forbidden unless we consider $m_\mu \neq 0$. Obviously, even in the last case, the decay will not happen easily, but it will take an amount of time.
The pion also admits another decay channel: $\pi^- \to e^- + \nu_e$. From the kinematics this decay is more favored because, since the electron mass is smaller than the muon, there is more possibility of spacing in the momentum and therefore there is a larger phase space. However, nature still prefers decay in the muon because $m_\mu > m_e$ therefore the muon violates the condition on the helicity. If both the two masses were zero then the pion would be stable, but this is not observed experimentally.
The other element to consider is the decay of the muon

$$\mu^- \to e^- + \bar\nu_e + \nu_\mu \qquad (1.13)$$

In the CM of the muon, in order to have the maximum momentum for the electron, there is a need for neutrinos to be emitted parallel and both to be opposed to the maximum momentum of the electron. Since the muon neutrino helicity is -1 and the helicity of the electronic antineutrino is +1, then the sum of their spins must be 0. Therefore, we deduce that the spins of the muon and the electron coincide. Thus, there may be two cases Fig.(1.2):
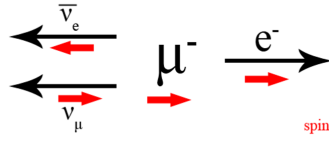
(a)
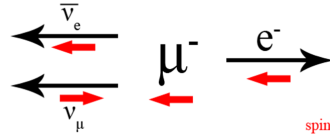
(b)

Figure 1.2: Possible ways muon's decay in electron with positive and negative helicity.

If the mass of the electron were 0, only case (b) occurs, since the massless leptons have helicity -1. Clearly the case (a) can always happen but the probability is very small. It is therefore deduced that, in the laboratory system, if one observes a high energy electron it is very probable that its direction is antiparallel to the muon's spin. Suppose you have a bundle of polarized muons of charge $q = Qe$ and make them interact with a magnetic field. Besides the precession of the magnetic moment with cyclotron frequency $\omega_c = -\frac{QeB}{m\gamma}$ also the spin precedes with a frequency $\omega_s = -\frac{gQeB}{2m} - \frac{(1-\gamma)Qeb}{m}$. Then defining $\omega_a \equiv \omega_s - \omega_c$ we have

$$\omega_a = -\frac{\left(\frac{g-2}{2}\right)QeB}{m} \equiv -\frac{aQeB}{m} \qquad (1.14)$$

where a is the anomaly discussed above.

If g were equal to 2 then the spin would remain anchored to the impulse, instead if $g > 2$ then $a_\mu \neq 0$ therefore the spin would rotate faster than the momentum. It has been previously observed that e^- has memory of the spin of μ^-. In the system of the rotating muon, therefore, it can be seen
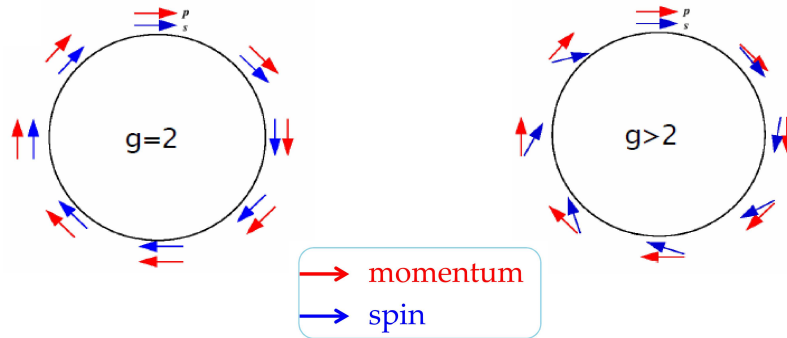
Figure 1.3: Muon's spin precession.

how, while he is still rotating, his spin is rotating faster (Fig. 1.3): when the spin is disposed in the opposite direction of the muon's momentum then the decay will be favored. It is therefore understood that, without making the muon beam interact with a magnetic field B, the helicity is fixed at +1 and the decay will have probability close to zero of future. [4]

1.3   The Muon g-2 Experiment

In the Muon g-2 experiment, how is shown in the figure (1.4), a very tight proton package over time is made to hit a target in order to obtain the pions that are used for the decay. The muons produced will be stored in a special ring in which there are 24 calorimeters and some electric quadrupoles that keep the focused beam.

Now, the total number of decay electrons decreases exponentially because
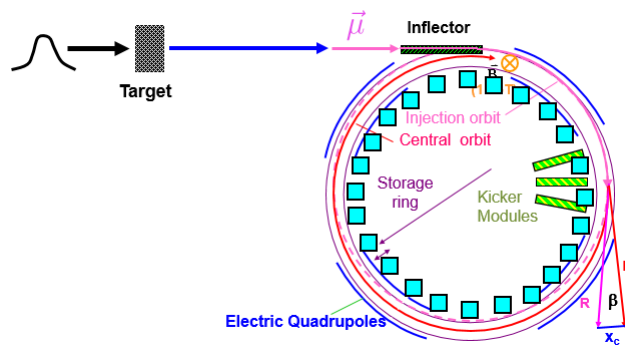
Figure 1.4: The g-2 experiment's ring.

the number of muons inside the ring exponentially decreases. In order for the beam to be on a circular orbit, an electric field is also needed to hold it

and to avoid divergence. It can be shown that

$$\vec{\omega}_a = -\frac{Qe}{m}\left[a\vec{B} - \left(a - \frac{1}{\gamma^2 - 1}\right)\left(\frac{\vec{\beta} \wedge \vec{E}}{c}\right)\right] \tag{1.15}$$

If we appropriately choose the muon's beam in such a way that $\gamma \approx 29.3$ and $p_\mu = 3.09\,GeV/c$ and the second term will be ignored and we get

$$\vec{\omega}_a = \frac{ea_\mu\vec{B}}{m} \tag{1.16}$$

This technique is called the magic moment approach. Measuring the anomaly is then reduced to the measurement of the magnetic field B and the measurement of the frequency of oscillation ω_a.

The magnetic field B could be measured with extreme precision, it is known that the magnetic field which on average interacts with the muon's beam is the average weighted with the distribution of muons in space:

$$< B >= \int M(r;\theta)B(r,\theta)drd\theta \tag{1.17}$$

where $B(r,\theta)$ can be calculated as multipole development:

$$B(r,\theta) = \sum_{n=0}^{\infty} r^n[c_n cos(n\theta) + d_n sen(n\theta)] \tag{1.18}$$

while the distribution of muons $M(r,\theta)$ is a function of the momentum:

$$M(r,\theta) = \sum_{m=0}^{\infty} k_m(r)cos(m\theta) + \sigma_m(r)sen(m\theta)] \tag{1.19}$$

Since $cos(m\theta)$ and $sin(m\theta)$ are orthogonal functions, the integral will be non-zero only with products of the same order; consequently, to minimize the uncertainty on $\langle B \rangle$, it is convenient to modulate the field so that the first orders of the development count more than the following ones. For this reason we try to have an almost constant magnetic field. For the purposes of the measurement, then, the magnetic field is analyzed by NMR (Nuclear Magnetic Resonator).

The oscillation frequency ω_α measure is done through the study of the muon's decay, as previously described. The theoretical principle is therefore very simple, but the experimental procedure presents various difficulties. The muon's average life is in fact very low $\tau_\mu = 2.2\mu s$ and in this short period muons must be produced by the pion decay, trapped in a magnetic field and their spin must be analyzed. However, it is possible to extract a dependency on ω_α by selecting only the electrons that have maximum energy in the lab, about 3.1 GeV. In fact, the latter will be precisely those electrons

that, in the muon's resting reference system, have about 53MeV energy, and we have seen that the latter tend to be emitted in the opposite direction to the muon's spin. Thus, the number of maximum-energy electrons reaches a maximum when the muon's spin is antiparallel to its momentum, and a minimum when the muon's spin is parallel to its momentum; in fat, since the spin rotates with respect to the moment with velocity ω_α, also the number of maximum energy electrons will be modulated with this frequency. Since ω_α does not depend on time, the angle between the muon's spin and its momentum will have a trend of $\omega_\alpha t + \phi$ with ϕ constant. In the absence of any background noise due to instruments, the spectrum of the muon population decay is described by the following functional form:

$$f(t) = N_0 e^{-\lambda t} \left[1 + A\cos(\omega_a t + \phi)\right] \tag{1.20}$$
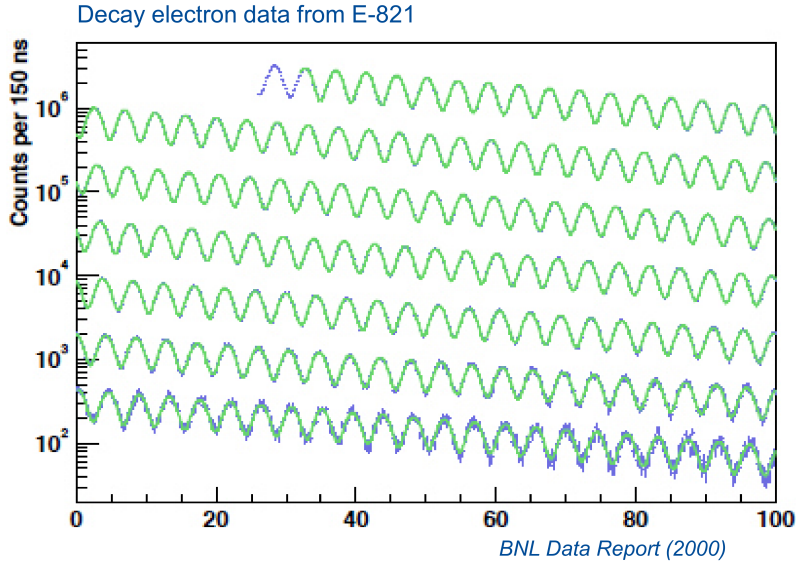

Figure 1.5: Functional form of the muon population in the decay.

From the figure (1.5) we can clearly see the exponential trend of the average life of the muon modulated by the precession of the spin. The peaks are separated by a period of about $149\,ns$. Fitting the long sinusoid $700\,\mu s$ (modulated with the exponential descending) with the equation (1.20) we can estimate A and ω_a. If we consider the Larmor precession of a non-relativistic charge in the same magnetic field, it will be equal to

$$\omega_L = -\frac{eB}{m} \tag{1.21}$$

and then we have

$$\alpha_\mu = \frac{\omega_\alpha}{\omega_L - \omega_\alpha} \tag{1.22}$$

If we divide numerator and denominator for ω_e, the frequency of Larmor precession related to electrons still immersed in the same magnetic field B, we can rewrite α_μ in terms of $R = \frac{\omega_\alpha}{\omega_e}$ and $\lambda = \frac{\omega_L}{\omega_e}$:

$$\alpha_\mu = \frac{R}{\lambda - R} \tag{1.23}$$

Since λ does not depend on the magnetic field B (since both ω_L and ω_e are proportional to it), it is possible to derive it from a different experiment, studying the hypertonic structure of the muonium. So measuring ω_e goes back to the value of R and then to α_μ. The Brookhaven experiment reported a value of the muon's magnetic anomaly equal to $\alpha_\mu = 11659208.0(6.3) \times 10^{-10}$.

Once the theoretical and experimental estimations have been obtained, one can proceed to the calculation of

$$\Delta\alpha_\mu = \alpha_\mu{}^{esp} - \alpha_\mu{}^{SM} = (260 \pm 78) \times 10^{-11} \tag{1.24}$$

This is a very important result especially because, although the theoretical calculation is extremely accurate, the measure of $\Delta\alpha_\mu$ is not comparable with 0. Therefore if we repeat this experiment trying to minimize experimental errors and the same result is obtained again, then there would be a definitive confirmation of the incompleteness of the Standard Model. For this reason it was set up at Fermilab, transporting and reusing the same accumulation ring of the E821 experiment, the experiment E989 for a new measure of $g - 2$. The experiment is in data collection and on 11 May it reached the same Brookhaven statistics. In 2 years we aim to accumulate a statistic 20 times greater than the E821 experiment. Fermilab's experiment presents new tools that allow a reduction in experimental uncertainty. In fact, 24 calorimeters are used in a 6x9 matrix with PbF_2 crystals read by a SiPM that have good spatial and temporal segmentation and reduce the pileup (two or more low energy electrons that accumulate being detected as a high energy electron). SiPM signals are recorded as a waveform by a waveform digitizer, which samples the signal at a frequency of 800MHz: a high sampling rate is crucial because the signal integral is the energy of the decay electron. Data acquisition tries to discard any pileups by eliminating double-peak signals. In addition, 3 tracker systems or 1500 straw trackers channels are used to monitor the spatial distribution of the beam. Finally, due to the very high number of decay electrons at the initial instant, the detectors do not respond uniformly, but at the beginning of the acquisition they have a reduction of the gain which would result in an excessively high systemic uncertainty; for this reason, a laser calibration system is employed which therefore deals with checking the stability in G gain of the system. The goal is to monitor the gain fluctuations of the calorimeter detectors to keep the systematic uncertainties due to the gain at around $0.02\,ppm$. For

this purpose a reference pulse is sent in such a way as to verify how the detector responds: the problem lies in doing it at very high precision. In particular, it has been estimated that in order to achieve the aim of the experiment it is necessary to keep systematic errors due to the fluctuation of the gain per thousand on the complete cycle of $700\,\mu s$. In reality, the need to control fluctuations is both short-term, that is, in the arc of a fill of $700\,\mu s$ (caused by rate of particles that induce over / under voltage), and in the long term in which case they are caused by changes in external conditions (temperature, day / night drift, etc.).[3] [5]

Chapter 2

Laser calibration system

The laser calibration system is used for calorimeters calibration. The laser sends pulses that are monitored through a series of optical and electronic components. It is desired that the response of the calorimeters is calibrated with precision relative to the level of per-thousand to obtain (in the E989 experiment) an accuracy of the results measured at the level of ppb (parts per billion). The pulses are emitted towards the active crystals of the 24 calorimeters through a complex system of sources and optical fibers. The radiation must be stable in intensity and timing to correct systemic fluctuations in the data measured by the calorimeters. It is also necessary a photodetector system inside the calibration architecture itself to monitor any fluctuations in the light along the optical path, which may be caused by mechanical vibrations or aging of the instrumentation. The main role is played by the Laser Control Board (LCB, electronic control board), which deals with pulse generation and time control for electronic components. The
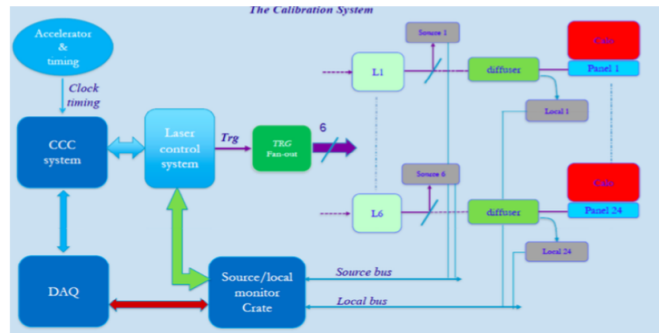

Figure 2.1: Laser calibration system's scheme.

figure (2.1) shows a sketch of the laser calibration system. The light source comes from six identical laser diodes with an average power of $20\,mW$ a pulse width of $700\,ps$ at a wavelength of $405 \pm 10\,nm$. The laser specifications give a power stability of 1% RMS, of 3% peak-peak on a 12-hour scale.

Each laser provides light to four calorimeters, meaning that each laser beam is divided into four lines focused on long quartz optical fibers. The output of each fiber is transmitted through a diffuser that uniformly illuminates a bundle of optical fibers. Each individual fiber of the beam provides light to a single calorimeter crystal. [2] Along its path towards the crystals, the light is monitored twice, the first time at the exit from the laser (Source Monitor, SM), another time at the arrival point (Local Monitor, LM) sending a fiber to the laser hut and comparing its output pulse with a reference pulse given by the SM. Some specific photo detectors deal with this process and the corresponding electronics have been designed to read, process and digitize the corresponding signals. Furthermore, these electronic components supply the power supply voltage to the photodetectors, read the different temperatures (ambient, on the preamplifier and on the board itself) and, at the end, stabilize the performance of the reading channel. The electronics, in fact, is able to independently generate pulses of known amplitude and send them to the input of the reading channel, which means that it has self-calibration capability. The laser must be used in two distinct ways. The first one is enabled, during the physical event, to correct the systematic variation of the SiPM gain caused by the high decay rate of the muon at the beginning of a filling cycle. The second one is dedicated to the simulations, without beam, to stimulate the detector and the DAQ with time sequences of specific laser pulses and to study the SiPM response to the double pulses. Furthermore, the laser is used for the time alignment of the SiPM in a calorimeter and between the heats themselves. [1] As a result, the LCB allows:

1. Calibration or pulse generation mode at programmable frequencies superimposed on the physical data provided in a $700\,\mu s$ muon fill. To homogeneously sample the SiPM gain at different points with muon filling of $700\mu s$ and reducing pileup events, the pattern can be moved at each fill of a fraction of the pulse period. The number of samples at each point is determined with a relative calibration error of 10^{-4}. Considering the number of photons in each pulse, the repetition frequency of muon filling and the frequency of calibration pulses within the $700\,\mu s$ window, we expect a few thousand samples at each point to be sufficient to achieve the required accuracy. This translates into an ability to calibrate the entire detector in one to two hours.

2. The simulation of the physical event that involves the activation of the laser according to the exponentially decreasing time function $e^{-t/\tau}$, as expected in the experiment due to the decay of the muon. In fact, an essential feature of the LCB is the ability to generate pulses or laser activation, based on any temporal distribution. This mode provides flexible SiPM tests to determine, for example, response linearity and gain stability. It also allows completely realistic tests of the reading electronics, DAQ and laser processing, based on any time distribution.

3. Synchronization of detectors and electronics providing a reference pulse on request or in connection with the signals of an accelerator machine.
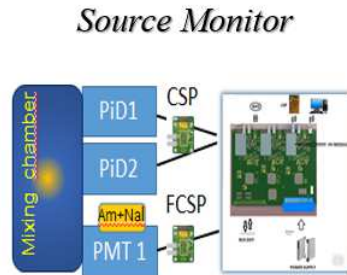
2.1   The Source Monitor

Figure 2.2: Source Monitor's structure.

The monitors are built with the aim of filtering any instabilities of the laser system: assuming that the incoming signal (recorded by the monitor) and the one produced by the calorimeters as an impulse response have the same fluctuation due to the laser, their ratio eliminates oscillation and returns information only on the instabilities of the calorimeter response. In particular, the purpose is to study the correlations of the signal with environmental parameters. As can be seen from the figure, the SM consists of:

- a Mixing Chamber, which takes care of collecting the light, making it a sort of photon gas and sorting it into the holes where the PiD and the PMT are hooked. The light that arrives will be proportional to the area of the holes: in particular that of the PMT is smaller because it has the function of an amplifier;

- two Pin Diodes (PiD1 and PiD2). The PiN diode S3589-08 features a very high response time and high photo efficiency. This component is used to verify the presence of fluctuation in the source. The use of two diode PINs for each monitor has been designed to filter any malfunction of one of the two;

- PMT H5783-04 which receives the pulses emitted by the photocathode mixing chamber. Its amplifier capacity highlights any fluctuations to which the pins are not sensitive;

- Am + NaI. Small impulses are emitted from an Americium source, which is the absolute reference for correcting the instability of the

PMT. As for Sodium Iodide, this has instead a function of organic scintillator.

- Finally, the signals will be amplified by the CSP and the FCSP and then go on a card that acquires data and sends them to the PC.
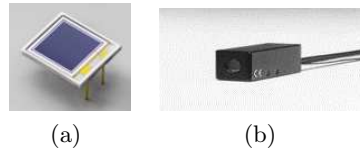

(a) (b)

Figure 2.3: Source Monitor's components: PinDiode S3589-08 (a), PMT H5873-04 (b).

The two PIN diodes, given their low gain, have a weak dependence on temperature and bias voltage, due in large part to the electronics with which the output signal is read. The main fluctuation that is perceived is the intrinsic fluctuation of the source. A joint analysis of both signals allows to isolate the intrinsic variation and to go back to a first estimate of the oscillations of the source. On entry to the PMT, however, a much smaller number of photons is sent, and the amplification also accentuates the oscillations due to temperature and electronics. The comparison in this case is made between the input signal from the mixing chamber and the signal of the Americium. The fluctuations of the latter depend only on the electronics (and through it also by the temperature), and a comparison of the two signals once again allows to isolate the intrinsic variation of the source.
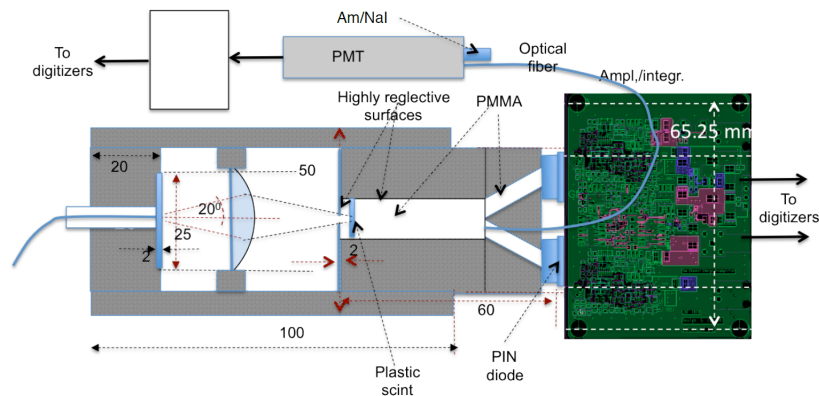

Figure 2.4: Source Monitor's prototype scheme.

A representation of the source monitor prototype is given in Fig 2.4 . The light enters from the left through the optical fiber and is diffused with an opening of 20 degrees. The diffused ray is then concentrated on

a scintillator disk and brought into the mixing chamber, based on PMMA. The scintillator acts as an ideal diffuser because it emits isotropically. The PMMA cavity, with its role as a mixing chamber, eliminates point fluctuations that can be produced during laser emission. The radiation from the mixing chamber is then brought into the two PIN diodes and the PMT. PIN diodes are relatively slow compared to the incoming signal (amplitude of about 10ns) but fast enough to interface with the integrated electronics. The PMT, on the other hand, operates at low voltage and produces its own HV. The laser fluctuations are eliminated in the relative evaluations of the detector outputs, allowing to analyze other possible instabilities of the apparatus or of the individual signals. The stability of the PMT is monitored independently with exposure to a radioactive source with known decay (about 10 events/s) of Am on a crystal of NaI, which acts as an absolute reference in first approximation.

Chapter 3

Data Analysis

The laser calibration system must be as stable as possible. In order for this to happen, the apparatus must be independent of external factors, however it will be shown that there are correlations between tool responses and external factors.

The experimental apparatus consists in fact:

- Source Monitor of the same type as the one described above, with two model S3589-08 diode PINs and a model PM5 H5783-04;

- Laser of 405 nm;

- PDL laser control system 200-B pulse diode laser;

- Thorlabs PM100USB power meter;

- Beam splitter.

The beam splitter simulates the behavior of the laser in the case of the E989 experiment. A part of the impulse (80%), in fact, is sent to the calorimeters for calibration, while the remainder (20 %) is sent to the Source Monitor for the study of the intrinsic oscillations of the source (Fig. 3.1). The data that has been analyzed, were collected at the Fermilab in May 2018, and count three sets, which will be referred to as "SM1", "SM3" and "SM6". The
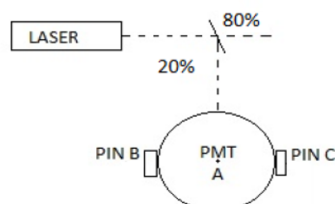
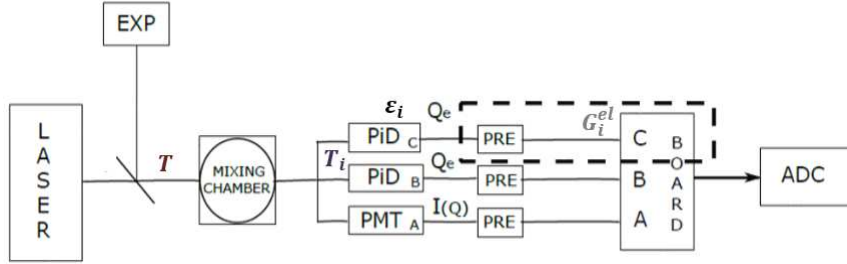Figure 3.1: Scheme of laser calibration system's part.

Figure 3.2: Photodetectors signals scheme.

ultimate aim is to try to decouple the fluctuations of the signals from the variables on which there is no direct control, such as the temperature of the preamplifier. This is achieved by direct study of the signals and subsequent analysis of the "corrected" signals, where to correct we mean the private signal of the fluctuation caused by the parameter studied.

Given the scheme in Fig. (3.2) it is possible to write the following relation:

$$S_{Mi} = N_\gamma T \frac{T_i}{T_B + T_C + \alpha} \epsilon_i G_i^{el} \tag{3.1}$$

where:

- N=number of incoming photons;

- T= transmission coefficient;

- T_B, T_C = PinDiode's transmission coefficient;

- α = infinitesimal quantity of photons detected by the PMT;

- ϵ_i = quantum efficiency;

- G_i^{el} = electronic gain;

3.1 Source Monitor 3

The analyzed data cover an interval of 30 days of May 2018 and the temporal profiles that we will show have a temporal binning such that each bin corresponds to about 10 minutes. It was chosen to show the analysis of the Source Monitor 3 as this results to have more significant results, being the separation between the signals of the Americium ADC and the Laser ADC better than the other Source Monitors analyzed.

3.1.1 PMT

As previously described, we obtain two distinct signals from the PMT: one deriving from the source of Americium (which we will indicate with Ame) and the other deriving from the laser source (which we will indicate with PMT). As can be seen in Fig. 3.3, the two signals are clearly distinguishable because the distributions of the two signals are mean values extremely different.
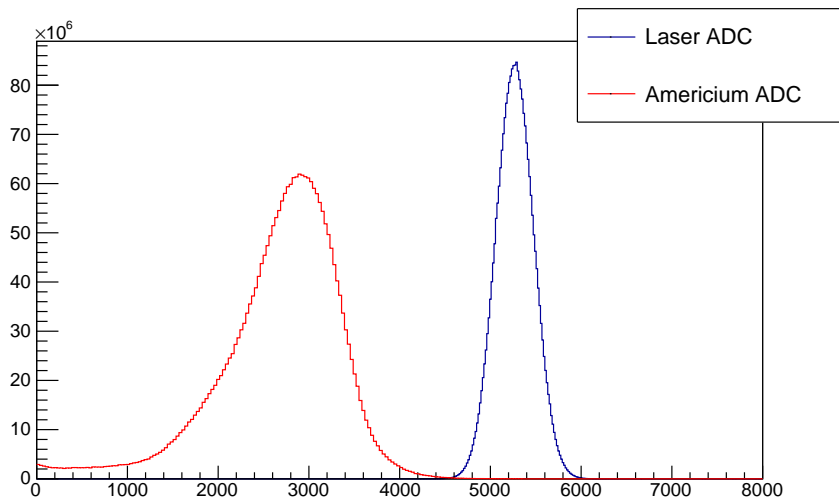

Figure 3.3: Americum ADC and Laser ADC distribution.

In Fig.3.4 time trends of the signals are shown. These signals do not appear
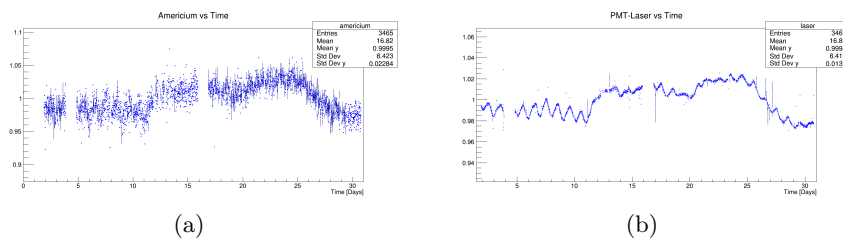
Figure 3.4: Americium (a) and Laser (b) ADC signals profile.

to be constant over time and present modulation. This trend can be linked to the fluctuation of the preamplifier temperature (CT). In Fig. 3.5 the trend of the temperature in the analyzed time range is shown.

The laser signal is strongly anticorrelated with the temperature as shown by Fig. 3.6.

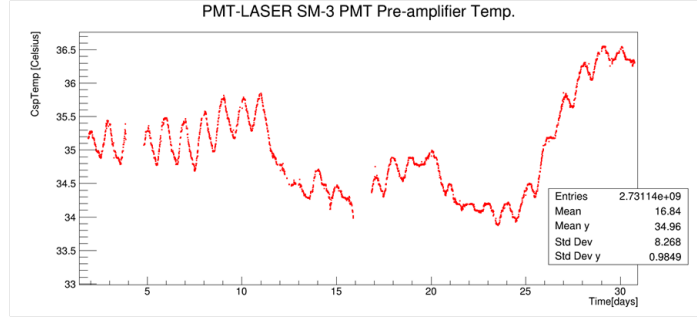To better understand how the signal is correlated with the tempera-

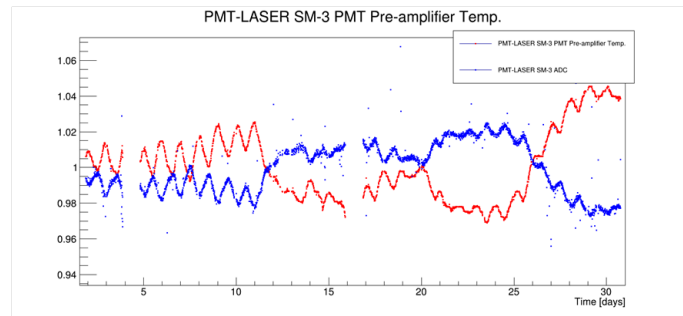Figure 3.5: Photomultiplier Csp temperature profile.

Figure 3.6: Csp temperature and ADC signal's pmt profiles.

ture the signal is shown as a function of it. The profile in Fig 3.7 shows two different linear trends, at low temperatures and at high temperatures. Each of the two intervals was fitted with a line so that the relative correlation coefficient can be extracted. The $p_1(LowTemperature)$ results to be higher than $p_1(HighTemperature)$. The same fit has been done for the Americium signals in function of the temperature and also in this case the correlation in the same way. The ADC signals were corrected as follows: $ADC'(t) = ADC(t) + p_1(T(t^*) - T(t))$ where ADC' is the correct signal, p_1 is the correlation coefficient obtained from the fit and $T(t^*)$ is the point of discontinuity that distinguishes the two trends (low temperature and high temperature). Obviously each of the two intervals has been corrected with the related correlation coefficient.

In Fig. 3.8 the comparison between the signals and the correct signals is shown. The Laser ADC has a really good correction while the Americium shows a not too effective correction. Consider the p_1 relative to the Laser ADC signal. The correlation with the temperature depends both on the variation in gain of the photomultiplier and on the variation of the laser
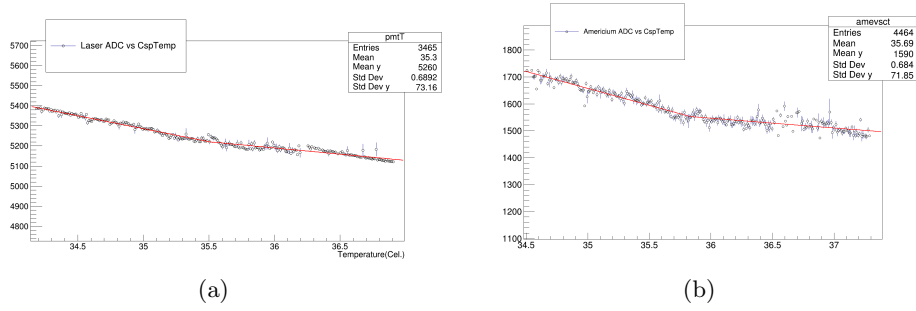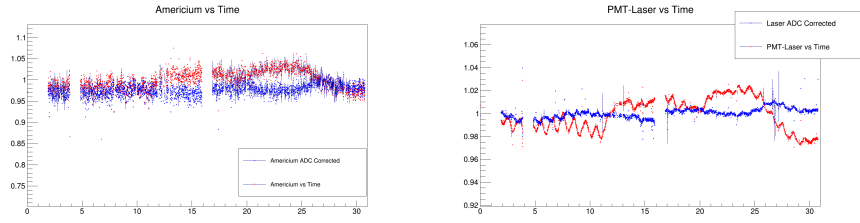
(a)   (b)

Figure 3.7: Linear Fit Pmt ADC vs CspTemp and Americium ADC vs CspTemp.

(a) *Americium ADC corrected and orig-*   (b) *Pmt ADC corrected and original*
inal Americium ADC.   *Pmt ADC.*

Figure 3.8: Source Monitor 3

source, to understand how each of these affects the variation of the signal of the ADC suppose to write:

$$p_1(LaserPMT) = p_1(source) + p_1(electronics)$$

consider $p_1(electronic) = p_1(ame)$ as we assume that the source of americium is uncorrelated by the temperature, in first approximation .
We want to see in which percentage the signal varies with respect to the mean value, separating the contribution of electronics from the source one. Consider the low temperature regime: $p_1(source) = p_1(LaserPMT) - p_1(Electronics) = 38.5 \frac{Counts}{\circ C}$. By dividing this last one by the mean value of the Laser ADC, the per cent variation of the counts per degree Celsius due to variations of the laser source occurs.

$$\frac{p_1(Source)}{ADC^*(Laser)} = \frac{\Delta Counts(Source)}{T} = 0,75\% \qquad (3.2)$$

This value is the same both for high temperatures and for low temperatures, this leads us to think that the different behavior in the two ranges is due to the electronics, also confirmed by the behavior of the Americium. Dividing the $p_1(electronic)$ for the mean value of the Laser ADC, we obtain that the

variation in gain of the electronics is:

$$\frac{p_1(Electronics)}{ADC^*(Laser)} = \frac{\Delta G}{G} \tag{3.3}$$

$$\frac{\Delta G}{G}(LowTemperature) = 1,8\% \tag{3.4}$$

$$\frac{\Delta G}{G}(HighTemperature) = 0,4\% \tag{3.5}$$

3.1.2   Pin Diode

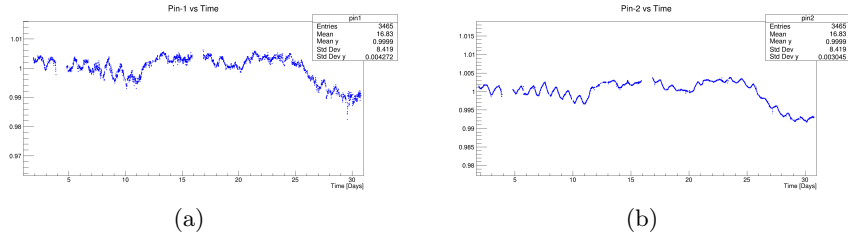Also the signals of the Pin Diodes are not constant over time as shown in fig 3.9.

Figure 3.9: Pin1 (a) and Pin2 (b) ADC signals profile.

The correlation with the preamplifier temperature shows a similar trend to that of the photomultiplier. However, in this case, p_1 (High Temp) is bigger than p_1 (Low Temp).
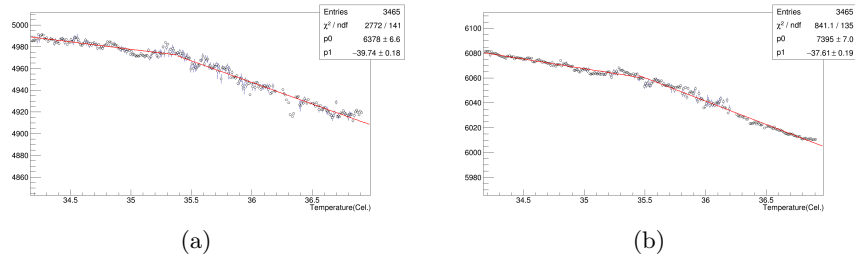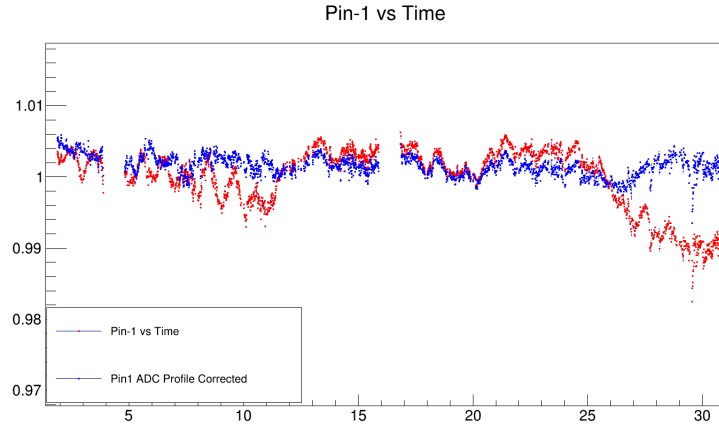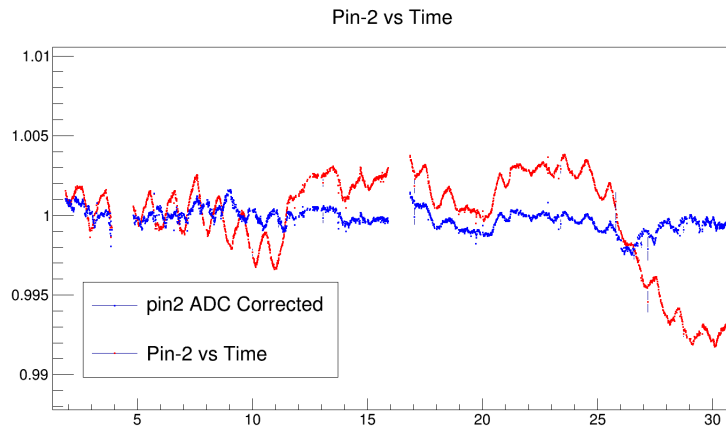

Figure 3.10: Linear Fit Pin1 ADC vs CspTemp and Pin2 ADC vs CspTemp.

The same type of corrections were also made in this case 3.11. These

(a) *Pin1 ADC corrected and original Pin1 ADC.*

(b) *Pin1 ADC corrected and original Pin1 ADC.*

Figure 3.11: Source Monitor 3

prove to be quite effective but there is still a residual modulation that will be the subject of future studies. In the table 3.12 is reported the values of p_1 expressed in $\frac{Counts}{^{\circ}C}$ of the whole analysis performed on the Source Monitor 3.

P$_1$ [#Counts/°C]	P$_1$ [LowTemp]	P$_1$ [HighTemp]
Pin1	-13,6±0,2	-38,9±0,2
Pin2	-15,5±0,2	-37,6±0,2
Laser	-132,9±0,2	-61,2±0,3
Americium	-94,4±0,2	-20,5±0,2

Figure 3.12: Source Monitor 3 data analysis results.

3.2 Source Monitor 1 and Source Monitor 6

The same type of analysis was done for the Source Monitor 1 and for the Source Monitor 6 with the same temporal range data. In both signals they appear to be anticorrelated with the preamplifier temperature. For the Pin Diodes p_1(High Temp) it always appears to be bigger than p_1 (Low Temp). However, because of the not good distinguishable of the two photomultiplier signals it is not always possible to see different trends in the two temperature regions and it is possible to extract a single correlation coefficient. This implies a lower relevance in the ΔG, derived from contamination between the two signals.

3.2.1 Source Monitor 1

In the tab3.13 the results of the source monitor 1 analysis are reported. Because of the previously described problems, the Americium signal has only a single correlation coefficient so we have that $\frac{\Delta G}{G}(LowTemperature) = \frac{\Delta G}{G}(HighTemperature) = 0,15\%$. In figure 3.14 the comparisons of the signals with the correct signals are shown. The corrections are quite good and consistent with those shown above.

P$_1$ [#Counts/°C]	P$_1$ [LowTemp]	P$_1$ [HighTemp]
Pin1	-22,2±0,2	-80,0±0,2
Pin2	-29,3±0,3	-73,7±0,2
Laser	-195,7±0,2	-302,7±0,2
Americium	-14,1±0,1	

Figure 3.13: Source Monitor 1 data analysis results.

(a) *Pin1 ADC corrected and original Pin1 ADC.*

(b) *Pin1 ADC corrected and original Pin1 ADC.*

(c) *Americium ADC corrected and original Americium ADC.*
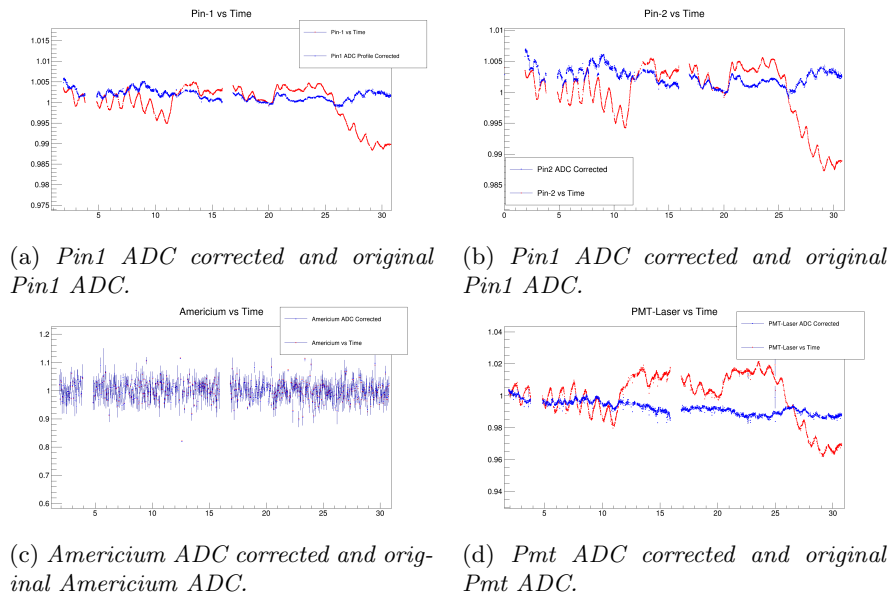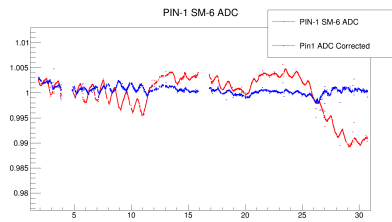
(d) *Pmt ADC corrected and original Pmt ADC.*

Figure 3.14: Source Monitor 1
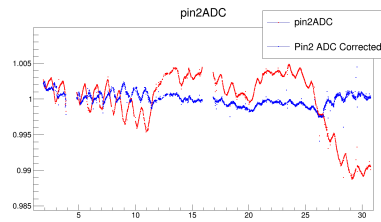
3.2.2 Source Monitor 6

In the tab 3.15 the results of the source monitor 6 analysis are reported. In this case we have just one value of p_1 for the Laser signal and we also have $\frac{\Delta G}{G}(LowTemperature) = 2,4\%$, $\frac{\Delta G}{G}(HighTemperature) = 0,7\%$. In figure 3.16 the comparisons of the signals with the correct signals are shown. The corrections are quite good and consistent with those shown above.

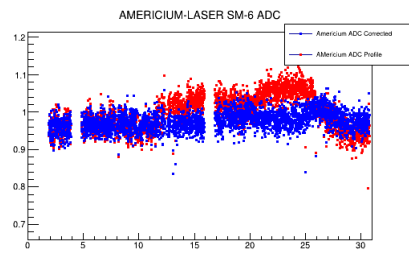| P_1 [#Counts/°C]	P_1 [LowTemp]	P_1 [HighTemp]
Pin1	-24,4±0,2	-68,1±0,2
Pin2	-32,0±0,2	-72,7±0,2
Laser	-167,4±0,1	
Americium	-125,6±0,3	-36,3±0,2

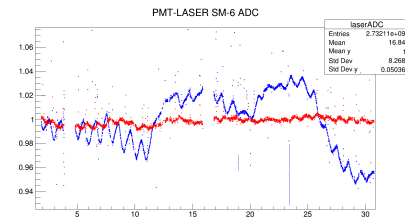Figure 3.15: Source Monitor 6 data analysis results.

(a) *Pin1 ADC corrected and original Pin1 ADC.*

(b) *Pin1 ADC corrected and original Pin1 ADC.*

(c) *Americium ADC corrected and original Americium ADC.*

(d) *Pmt ADC corrected and original Pmt ADC.*

Figure 3.16: Source Monitor 6

Conclusion

The analysis produced good results. As expected, the Source Monitors signals from the laser calibration system are anti-correlated with the preamplifier temperature. In all the Source Monitor analyzed, the electronics show different behaviors at high and low temperatures. For Pin Diodes, the correlation coefficient at high temperatures is higher than those at low temperatures. However, for the signals of the photomultiplier, Laser and Americium, when the impacts are distinguishable at the opposite, that is, the coefficient at low temperatures is greater than that at high temperatures. However if the signals of the photomultiplier are not well divisible the contamination between the two can hide this effect of the electronics. Other analyzes on a temporal range like this or even wider will be carried out to fully understand this new observed behavior.

Bibliography

[1] L. P. Alonzi et al. The calorimeter system of the new muon g -2 experiment at Fermilab. *Nucl. Instrum. Meth.*, A824:718–720, 2016.

[2] A Anastasi, A Basti, F Bedeschi, M Bartolini, G Cantatore, D Cauz, G Corradi, S Dabagov, G Di Sciascio, R Di Stefano, et al. Electron beam test of key elements of the laser-based calibration system for the muon g-2 experiment. *Nuclear Instruments and Methods in Physics Research Section A: Accelerators, Spectrometers, Detectors and Associated Equipment*, 842:86–91, 2017.

[3] JL Holzbauer et al. The muon g-2 experiment overview and status. *arXiv preprint arXiv:1712.05980*, 2017.

[4] F. Jegerlehner. The Muon g-2 in Progress. *Acta Physica Polonica B*, 49:1157, 2018.

[5] Marc Knecht. General discussion on g-2. *EPJ Web of Conferences*, 179:01008, 01 2018.